

Analysis of UAV Corridors in Cellular Networks

Saeed Karimi-Bidhendi*, Giovanni Geraci[‡], and Hamid Jafarkhani*

*Center for Pervasive Communications and Computing, Univ. of California, Irvine CA, USA

[‡]Universitat Pompeu Fabra (UPF), Barcelona, Spain

Abstract—In this article, we introduce a new mathematical framework for the analysis and design of UAV corridors in cellular networks, while considering a realistic network deployment, antenna radiation pattern, and propagation channel model. By leveraging quantization theory, we optimize the electrical tilts of existing ground cellular base stations to maximize the coverage of both legacy ground users and UAVs flying along specified aerial routes. Our practical case study shows that the optimized network results in a cell partitioning that significantly differs from the usual hexagonal pattern, and that it can successfully guarantee coverage all over the UAV corridors without degrading the perceived signal strength on the ground.

I. INTRODUCTION

Barely seen in action movies until a decade ago, the progressive blending of uncrewed aerial vehicles (UAVs) into our daily lives will enhance safety and greatly impact labor and leisure activities alike. Most stakeholders regard reliable connectivity as a must-have for the UAV ecosystem to thrive. As a result, UAV cellular communications have witnessed a surge of interest in terms of (i) what networks can do for UAVs and (ii) what UAVs can do for networks [1]–[5].

As for (i)—focus of the present paper—the mobile industry and its academic research counterpart have long joined forces to pursue reliable connectivity up in the air by re-engineering existing terrestrial networks, originally designed for ground users only [6], [7]. Recent ideas for ubiquitous aerial connectivity hinge, e.g., on network densification [8]–[12], dedicated infrastructure for aerial services [13], [14], or leveraging satellites to complement the ground network [15], all requiring costly hardware or signal processing upgrades.

Fortunately, many impactful UAV use cases could still be enabled by providing reliable connectivity along predetermined aerial routes, i.e., *UAV corridors*, enforced by the appropriate traffic authorities [16], [17]. The research community has started contributing in this direction by studying UAV trajectory optimization, e.g., matching the route of a UAV to the best coverage pattern provided by the network [18]–[21]. More recent work has targeted tuning cellular deployments to cater for UAV corridors through system-level simulations, large-scale optimization, or the theoretical analysis of a simplified setup [22]–[25]. However, there is an unmet need for a general mathematical framework allowing the analysis and design of UAV corridors in cellular networks.

This work was supported in part by the NSF Award CNS-2229467 and by the Spanish State Research Agency through grants RTI2018-101040-A-I00, PID2021-123999OB-I00, and through the “Ramón y Cajal” program.

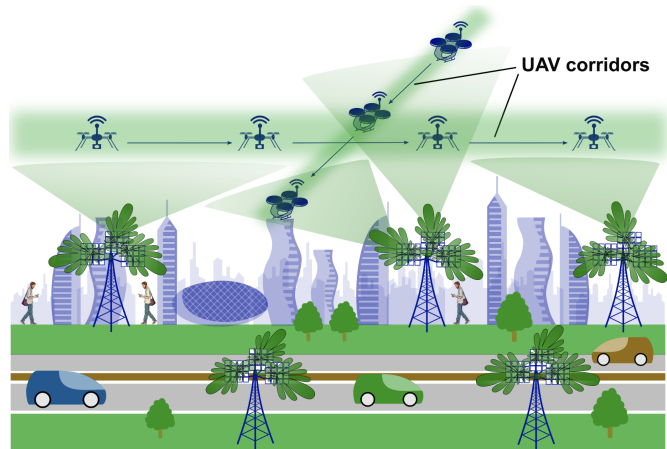


Fig. 1: Illustration of a cellular network with downtilted and uptilted base stations providing coverage to ground users as well as UAVs flying along corridors (blurred green).

In this paper, we take the first step towards creating such mathematical framework through quantization theory [26]–[32]. Specifically, we determine the necessary conditions and design an iterative algorithm to optimize the antenna tilts at each base station of a cellular network for a maximum received signal strength (RSS)—a proxy for coverage—at both legacy ground users and UAVs flying along corridors. To the best of our knowledge, this is the first work doing so in a rigorous yet tractable manner, while accounting for a realistic network deployment, antenna radiation pattern, and propagation channel model. We further put our mathematical framework into practice with a case study, whose main takeaways can be summarized as follows:

- Pursuing satisfactory coverage of both ground users and UAV corridors can result in a highly uncustomary cell partitioning that profoundly differs from a hexagonal pattern, commonplace in legacy ground-only systems.
- By tilting up a selected subset of base stations, one can significantly boost the RSS along multiple UAV corridors compared to an all-downtilt baseline, achieving levels of aerial coverage close to an upper bound arrangement that ignores legacy ground users altogether.
- Additionally, one can nearly preserve the quality coverage on the ground, maintaining levels of RSS close to those experienced in a scenario devoid of UAVs.

II. SYSTEM MODEL

The set-up under consideration is illustrated in Fig. 1 and detailed as follows.

A. Network Topology

1) *Ground cellular network*: The backbone of our network is a ground cellular deployment comprising N base stations (BSs) that provide coverage and service for network users. For each $i \in \{1, \dots, N\}$, we denote the height and 2D location of BS i by $h_{i,B}$ and p_i , respectively. Let $\theta_i \in [-90^\circ, +90^\circ]$ be the vertical antenna tilt of BS i , which can be optimized by a mobile operator, with positive and negative angles denoting uptilts and downtilts, respectively. Let $\phi_i \in [-180^\circ, +180^\circ]$ be the antenna horizontal boresight direction (azimuth) of BS i , assumed fixed given the deployment.

2) *UAV corridors and legacy ground users*: Our network entails two types of users: UAVs and ground-users (GUEs). UAVs traverse a 2D region $Q_U = \bigcup_{u=1}^{N_U} Q_u$ consisting of N_U UAV corridors Q_u , i.e., predefined 2D aerial regions. For each corridor Q_u , all UAVs are assumed to fly at the same height h_u . Ground users (GUEs) populate a 2D region Q_G and have a fixed height h_G . Let $\lambda(q)$ be a probability density function that reflects the distribution of users in $Q = Q_U \cup Q_G$. Each user in Q is associated with the BS providing the largest received signal strength (RSS), defined in the sequel. Hence, the region Q can be partitioned into N different subregions $\mathbf{V} = (V_1, \dots, V_N)$ such that users in V_i are associated with BS i .

B. Channel Model and Performance Metric

1) *Antenna gain*: We assume BSs equipped with directional antennas. The vertical and horizontal half-power beamwidths of the directional antennas are denoted by θ_{3dB} and ϕ_{3dB} , respectively. The total antenna gain of BS i in dB is given by

$$A_{i,q} = A_{\max} + A_{i,q}^V + A_{i,q}^H, \quad (1)$$

where A_{\max} denotes the maximum antenna gain at the boresight, $A_{i,q}^V$ and $A_{i,q}^H$ denote the vertical and horizontal antenna gains in dB, respectively, given by [33]

$$A_{i,q}^V = -\frac{12}{\theta_{3dB}^2} [\theta_{i,q} - \theta_i]^2, \quad (2)$$

$$A_{i,q}^H = -\frac{12}{\phi_{3dB}^2} [\phi_{i,q} - \phi_i]^2. \quad (3)$$

The vertical antenna gain $A_{i,q}^V$ in (2) depends on the vertical tilt θ_i of BS i and on the elevation angle $\theta_{i,q}$ between BS i and user location $q \in Q$, calculated as

$$\theta_{i,q} = \tan^{-1} \left(\frac{h_q - h_{i,B}}{\|q - p_i\|} \right), \quad (4)$$

where $\|\cdot\|$ denotes l^2 norm. The horizontal antenna gain $A_{i,q}^H$ in (3) depends on the difference $[\phi_{i,q} - \phi_i] \in [-180^\circ, +180^\circ]$,

where ϕ_i is the azimuth orientation of BS i and $\phi_{i,q}$ is the azimuth angle between BS i and user location q , given by

$$\phi_{i,q} = \begin{cases} \tan^{-1} \left(\frac{q_y - p_{i,y}}{q_x - p_{i,x}} \right) + 180^\circ \times 2c & \text{if } q_x - p_{i,x} > 0 \\ \tan^{-1} \left(\frac{q_y - p_{i,y}}{q_x - p_{i,x}} \right) + 180^\circ \times (2c+1) & \text{if } q_x - p_{i,x} < 0 \end{cases} \quad (5)$$

where subscripts \cdot_x and \cdot_y denote the horizontal and vertical coordinates of a point, respectively, and the integer c is chosen in a way that $-180^\circ \leq \phi_{i,q} - \phi_i \leq +180^\circ$.

2) *Pathloss*: The distance-dependent pathloss between a user at location q and BS i is given by

$$L_{i,q} = a_q + b_q \log_{10} \left[\|q - p_i\|^2 + (h_q - h_{i,B})^2 \right]^{\frac{1}{2}}, \quad (6)$$

where for each user location q , the constants a_q and b_q depend on the carrier frequency and on the pathloss exponent, the latter affected by the BS deployment features, the height of the user at q and the link's line-of-sight (LoS) condition. In our numerical simulations, we employ practical values for the parameters a_q and b_q , obtained from [6], [33] and reported in Section IV-B.

3) *Received signal strength*: The RSS in dBm from BS i at user location q is given by¹

$$\begin{aligned} \text{RSS}^{(i)}(q; \theta_i) &= \rho_i + A_{i,q} - L_{i,q} \quad [\text{dBm}] \\ &= \rho_i + A_{\max} - \frac{12}{\theta_{3dB}^2} [\theta_{i,q} - \theta_i]^2 - \frac{12}{\phi_{3dB}^2} [\phi_{i,q} - \phi_i]^2 \\ &\quad - a_q - b_q \log_{10} \left[\|q - p_i\|^2 + (h_q - h_{i,B})^2 \right]^{\frac{1}{2}}, \quad [\text{dBm}] \end{aligned} \quad (7)$$

where ρ_i denotes BS i 's transmit power measured in dBm.

C. Performance Function

In the remainder of the paper, we assume that all BS locations p_i and azimuth orientations ϕ_i are fixed while all BS vertical antenna tilts θ_i are optimized. Our main goal is to maximize the provided received signal strength averaged over all users in the network.

Remark 1. *Optimizing the vertical tilts θ_i entails that each BS has a different value of θ_i and therefore a different received signal strength $\text{RSS}^{(i)}(q; \theta_i)$. Moreover, the latter is not necessarily a non-increasing function of the distance $\|q - p_i\|$, e.g., moving away from a BS can sometimes yield a worse pathloss $L_{i,q}$ but a better antenna gain $A_{i,q}$.*

The overall performance function, i.e., RSS in dBm averaged over all users in the network, is given by:

$$\Phi(\mathbf{V}, \Theta) = \sum_{i=1}^N \int_{V_n} \text{RSS}^{(i)}(q; \theta_i) \lambda(q) dq. \quad (8)$$

Our goal is to optimize the performance function $\Phi(\mathbf{V}, \Theta)$ over the cell partitioning $\mathbf{V} = (V_1, \dots, V_N)$ and BS vertical antenna tilts $\Theta = (\theta_1, \dots, \theta_N)$. Note that, while other choices for $\Phi(\mathbf{V}, \Theta)$ are not precluded, averaging the RSS in dBm—i.e., in logarithmic scale and thus equivalent to a max-product

¹While our analysis is general and can incorporate shadow fading, we here neglect it to focus on the role played by optimizing the vertical tilts θ_i .

criterion in linear units—pursues fairness among users, as it will be shown in our case study.

III. ANALYTICAL FRAMEWORK

As shown in (8), the performance function Φ depends on both variables \mathbf{V} and Θ ; thus, our goal is to find the optimal cell partitioning $\mathbf{V}^* = (V_1^*, \dots, V_N^*)$ and vertical antenna tilts $\Theta^* = (\theta_1^*, \dots, \theta_N^*)$ that maximize the performance function. Note that not only the variables \mathbf{V} and Θ are interdependent, i.e., the optimal value for each variable depends on the value of the other variable, but also this is an NP-hard optimization problem. Our aim is to develop an alternating optimization algorithm that iteratively updates the values of \mathbf{V} and Θ . We accomplish this goal in two optimal steps: (i) updating the cell partitioning \mathbf{V} for a given set of vertical antenna tilts Θ ; and (ii) updating the BS vertical antenna tilts Θ for a given cell partitioning \mathbf{V} . The following proposition provides the necessary condition and update rule for Step (i):

Proposition 1. *The optimal cell partitioning \mathbf{V}^* for a given set of vertical antenna tilts Θ is given by:*

$$V_n^*(\Theta) = \left\{ q \in Q \mid \text{RSS}^{(n)}(q; \theta_n) \geq \text{RSS}^{(k)}(q; \theta_k), \forall k \in \{1, \dots, N\} \right\}, \quad (9)$$

for each $n \in \{1, \dots, N\}$.

Proof. Given any arbitrary cell partitioning of Q such as $\mathbf{W} = (W_1, \dots, W_N)$, we have:

$$\Phi(\mathbf{W}, \Theta) = \sum_{n=1}^N \int_{W_n} \text{RSS}^{(n)}(q; \theta_n) \lambda(q) dq \quad (10)$$

$$\leq \sum_{n=1}^N \int_{W_n} \max_k \left[\text{RSS}^{(k)}(q; \theta_k) \right] \lambda(q) dq \quad (11)$$

$$= \int_Q \max_k \left[\text{RSS}^{(k)}(q; \theta_k) \right] \lambda(q) dq \quad (12)$$

$$= \sum_{n=1}^N \int_{V_n^*} \max_k \left[\text{RSS}^{(k)}(q; \theta_k) \right] \lambda(q) dq \quad (13)$$

$$= \sum_{n=1}^N \int_{V_n^*} \text{RSS}^{(n)}(q; \theta_n) \lambda(q) dq \quad (14)$$

$$= \Phi(\mathbf{V}^*, \Theta). \quad (15)$$

Thus, \mathbf{V}^* yields the maximum performance and is optimal. ■

Now, for the second step, we aim to find the optimal Θ^* that maximizes the performance function Φ for a given cell partitioning \mathbf{V} . Our approach is to apply the gradient ascent algorithm to find the optimal vertical antenna tilts. Gradient ascent is a first-order iterative optimization algorithm for finding a local maximum of a differentiable function. The idea is to take repeated scaled steps in the direction of the gradient since this is the direction of steepest ascent.

Proposition 2. *For each $n \in \{1, \dots, N\}$, the partial derivative of the performance function in (8) w.r.t. θ_n is given by*

$$\frac{\partial \Phi(\mathbf{V}, \Theta)}{\partial \theta_n} = \frac{24}{\theta_{3dB}^2} \left\{ \sum_{u=1}^{N_U} \int_{V_n(\Theta) \cap Q_u} (\theta_{n,q} - \theta_n) \lambda(q) dq + \int_{V_n(\Theta) \cap Q_G} (\theta_{n,q} - \theta_n) \lambda(q) dq \right\}. \quad (16)$$

Proof. The derivative of (8) contains two terms: (i) the derivative of the integrand, and (ii) the integral over the boundaries. According to (9), for a point q on the boundary of regions n and k , we have: $\text{RSS}^{(n)}(q; \theta_n) = \text{RSS}^{(k)}(q; \theta_k)$. Since the normal outward vectors at point q have opposite directions for these two regions, the term (ii) amounts to zero [26]. The gradient $\frac{\partial \Phi(\Theta)}{\partial \theta_n}$ is then given by the first term, obtained as:

$$\begin{aligned} \frac{\partial \Phi(\mathbf{V}, \Theta)}{\partial \theta_n} &= \int_{V_n(\Theta)} \frac{\partial}{\partial \theta_n} \text{RSS}^{(n)}(q; \theta_n) \lambda(q) dq \\ &\stackrel{(a)}{=} \frac{24}{\theta_{3dB}^2} \left\{ \sum_{u=1}^{N_U} \int_{V_n(\Theta) \cap Q_u} (\theta_{n,q} - \theta_n) \lambda(q) dq + \int_{V_n(\Theta) \cap Q_G} (\theta_{n,q} - \theta_n) \lambda(q) dq \right\}. \end{aligned} \quad (17)$$

where (a) follows from the definition of Q . ■

Propositions 1 and 2 provide the main ingredients to design the BS vertical antenna tilt (BS-VAT) optimization algorithm outlined in Algorithm 1.

Proposition 3. *The BS-VAT algorithm is an iterative improvement algorithm and converges.*

Proof. We demonstrate that none of the two steps in the BS-VAT algorithm decreases the performance function Φ in (8). In the first step, the cell partitioning \mathbf{V} is updated according to (9) while Θ is fixed. Proposition 1 indicates that the obtained \mathbf{V} is optimal for the current set of antenna tilts Θ . Thus, the first step does not decrease the performance function Φ . In the second step, the gradient ascent algorithm is utilized to optimize Θ while \mathbf{V} is fixed. Note that the learning rate at iteration t of the gradient ascent algorithm is equal to $\eta_t = \eta_0 \times \kappa^t$. Since $\sum_{t=1}^{\infty} \eta_t^2 < \sum_{t=1}^{\infty} \eta_t = \frac{\kappa}{1-\kappa} \eta_0 < \infty$, the gradient ascent is guaranteed to converge [34] and does not decrease the performance function Φ . Hence, the BS-VAT algorithm generates a sequence of non-decreasing performance function values. Since the performance function $\Phi(\mathbf{V}, \Theta)$ is also upper bounded because of the limited transmission power at each base station, the algorithm converges. ■

IV. CASE STUDY

To evaluate the performance of our theoretical framework, we consider a case study in this section.

Algorithm 1: BS vertical antenna tilt optimization

Result: Optimal BS vertical antenna tilts Θ^* and cell partitioning \mathbf{V}^* .

Input: Initial BS vertical antenna tilts Θ and cell partitioning \mathbf{V} , learning rate $\eta_0 \in (0, 1)$, convergence error thresholds $\epsilon_1, \epsilon_2 \in \mathbb{R}^+$, constant $\kappa \in (0, 1)$;

```

do
  Calculate  $\Phi_{\text{old}} = \Phi(\mathbf{V}, \Theta)$ ;
  # Update the cell partitioning  $\mathbf{V}$ ;
  for  $n \in \{1, \dots, N\}$  do
    | Update the cell  $V_n$  according to Eq. (9);
  end
  # Start the gradient ascent algorithm;
  Set  $\eta \leftarrow \eta_0$ ;
  do
    Calculate  $\Phi_s = \Phi(\mathbf{V}, \Theta)$ ;
    # Calculate the gradient  $\nabla_{\Theta} \Phi(\mathbf{V}, \Theta)$ ;
    for  $n \in \{1, \dots, N\}$  do
      | Calculate  $\frac{\partial \Phi(\mathbf{V}, \Theta)}{\partial \theta_n}$  according to Eq. (17);
    end
    # Update the learning rate;
     $\eta \leftarrow \eta \times \kappa$ ;
    # Update the vertical antenna tilts  $\Theta$ ;
     $\Theta \leftarrow \Theta + \eta \nabla_{\Theta} \Phi(\mathbf{V}, \Theta)$ ;
    Calculate  $\Phi_e = \Phi(\mathbf{V}, \Theta)$ ;
  while  $\frac{\Phi_e - \Phi_s}{\Phi_s} \geq \epsilon_1$ ;
  Calculate  $\Phi_{\text{new}} = \Phi(\mathbf{V}, \Theta)$ ;
while  $\frac{\Phi_{\text{new}} - \Phi_{\text{old}}}{\Phi_{\text{old}}} \geq \epsilon_2$ ;

```

A. Deployment Setup

Simulations are carried out for a practical cellular network consisting of 19 sites. Each site, say i , includes three sectors, i.e., three cells with the corresponding BSs placed at the exact same locations $p_{3 \times i - 2} = p_{3 \times i - 1} = p_{3 \times i}$ but with different azimuth orientations $\phi_{3 \times i - 2} = 0^\circ$, $\phi_{3 \times i - 1} = 120^\circ$, and $\phi_{3 \times i} = 240^\circ$. Thus, overall, there are $N = 57$ BSs with corresponding vertical antenna tilts to optimize. The BSs are placed on a hexagonal layout with inter-site distance $\text{ISD} = 500\text{m}$ as illustrated in Fig. 3. Site indices are provided in Fig. 3b. All BSs are assumed to have the same height and transmission power, with $h_{i,\text{B}} = 25\text{m}$ and $\rho_i = 43\text{dBm}$ $\forall i$, respectively. Ground users are distributed over a square area $Q_G = [-750, 750] \times [-750, 750]$ according to a uniform density function $\lambda_G(q)$ and are assumed to have the fixed height $h_G = 1.5\text{m}$. UAVs are distributed over $N_U = 4$ vertical aerial corridors, i.e., $Q_U = Q_1 \cup Q_2 \cup Q_3 \cup Q_4$, according to a uniform density function $\lambda_U(q)$. These corridors, shown in Fig. 3b, are located at $Q_1 = [-320, -280] \times [-400, 400]$, $Q_2 = [-120, -80] \times [-400, 400]$, $Q_3 = [80, 120] \times [-400, 400]$, and $Q_4 = [280, 320] \times [-400, 400]$ and their heights are set at $h_1 = h_4 = 150\text{m}$ and $h_2 = h_3 = 120\text{m}$. The density function $\lambda(q)$, which represents the distribution of users in $Q = Q_G \cup Q_U$, is a mixture of $\lambda_G(q)$ and $\lambda_U(q)$,

TABLE I: System-level parameters for our case study.

Deployment	
P	Hexagonal grid with intersite distance $\text{ISD} = 500$ m. Two tiers of BSs around the one at the origin, three sectors per site, 57 BSs in total, $h_{\text{B}} = 25$ m.
Q_U	Consisting of $N_U = 4$ aerial corridors
$Q_u, u = 1$	Vertical $[-320, -280] \times [-400, 400]$, $h_u = 150$ m
$Q_u, u = 2$	Vertical $[-120, -80] \times [-400, 400]$, $h_u = 120$ m
$Q_u, u = 3$	Vertical $[80, 120] \times [-400, 400]$, $h_u = 120$ m
$Q_u, u = 4$	Vertical $[280, 320] \times [-400, 400]$, $h_u = 150$ m
Q_G	Square area $[-750, 750] \times [-750, 750]$, $h_G = 1.5$ m
$\lambda_G(q), \lambda_U(q)$	Uniform in Q_G and Q_U , respectively
$\lambda(q)$	$\alpha \lambda_G(q) + (1 - \alpha) \lambda_U(q)$ with $\alpha = \{1, 0, 0.5\}$
Channel	
A_{max}, ρ_i	14 dBi, 43 dBm $\forall i$, respectively
$\theta_{3\text{dB}}, \phi_{3\text{dB}}$	$10^\circ, 65^\circ$, respectively
ϕ_i	Fixed for the three sectors: $\phi_i \in \{0^\circ, 120^\circ, 240^\circ\}$
a_q	$q \in Q_U$: 34.02 dB (carrier at 2 GHz)
	$q \in Q_G$: 38.42 dB (carrier at 2 GHz)
b_q	$q \in Q_U$: 22 (i.e., pathloss exponent 2.2)
	$q \in Q_G$: 30 (i.e., pathloss exponent 3.0)
Optimization	
Initial tilts	$\theta_i = 0 \forall i$
Initial partition	Each $q \in Q$ assigned to a random base station
$\eta_0, \kappa, \epsilon_1, \epsilon_2$	0.005, 0.999, 10^{-8} , 10^{-9} , respectively

i.e., $\lambda(q) = \alpha \lambda_G(q) + (1 - \alpha) \lambda_U(q)$ where α is the mixing ratio. In the sequel, we consider three values for the parameter α , namely 1, 0, and 0.5. These three values correspond to optimizing the cellular network for ground users only, for UAVs only, and for both, respectively.

B. Channel Setup

As per 3GPP specifications [6], [33], for a carrier frequency at 2GHz and LoS condition, the values of a_q and b_q are set as:

$$a_q = \begin{cases} 34.02 \text{ dB}, & \text{if } q \in Q_U, \\ 38.42 \text{ dB}, & \text{if } q \in Q_G, \end{cases} \quad (18)$$

$$b_q = \begin{cases} 22 \text{ (i.e., pathloss exponent 2.2)}, & \text{if } q \in Q_U, \\ 30 \text{ (i.e., pathloss exponent 3.0)}, & \text{if } q \in Q_G. \end{cases} \quad (19)$$

The vertical and horizontal half-power beamwidth of the directional antennas are set to $\theta_{3\text{dB}} = 10^\circ$ and $\phi_{3\text{dB}} = 65^\circ$, respectively. The maximum antenna gain at the boresight is set to $A_{\text{max}} = 14\text{dBi}$.

C. Vertical Antenna Tilt Optimization

The BS-VAT algorithm is initialized by a random cell partitioning, i.e., randomly assigning each $q \in Q$ to a base station, and setting $\theta_i = 0 \forall i$. The learning rate η_0 and constant κ are set to 0.005 and 0.999, respectively. The convergence error thresholds are set to $\epsilon_1 = 10^{-8}$ and $\epsilon_2 = 10^{-9}$.

Fig. 2 shows the optimal values of the vertical electrical antenna tilts θ_i^* for each cell in the three cases $\alpha = \{1, 0, 0.5\}$. As expected, $\alpha = 1$ (green) entails optimizing all antenna tilts for only legacy ground users, and thus results in downtilted

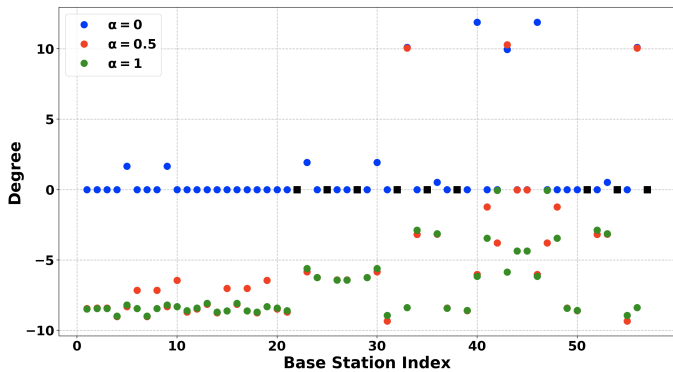


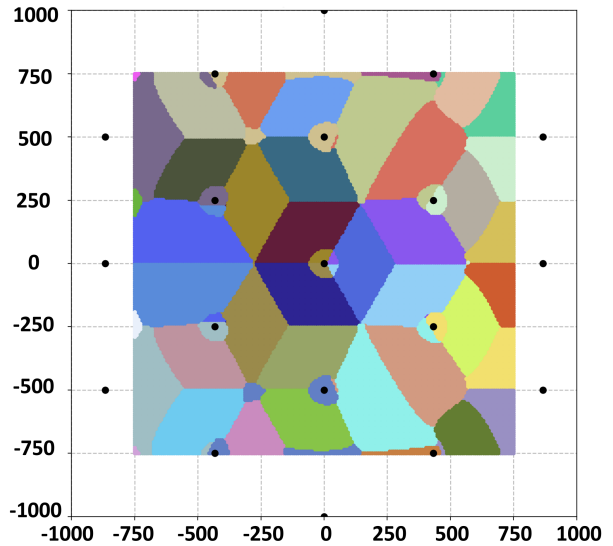
Fig. 2: Optimized vertical tilts θ_i^* for: ground users only ($\alpha = 1$, green), UAVs only ($\alpha = 0$, blue), and both ($\alpha = 0.5$, red). Black squares indicate cells that do not contribute to coverage.

BSs. Conversely, $\alpha = 0$ (blue) only caters for the four UAV corridors, and thus leads to uptilted BSs. As shown in Fig. 2, not all BSs effectively contribute to optimizing the performance function, resulting in some vertical tilts remaining at the initial value of zero. In particular, BSs 22, 25, 28, 32, 35, 38, 51, 54, and 57, that are shown by black squares in Fig. 2, do not contribute to the performance function in any of the three simulated scenarios of $\alpha = 0, 0.5$, and 1. Lastly, $\alpha = 0.5$ (red) seeks a coverage tradeoff between the ground and the UAV corridors, hence resulting in a small subset of BSs being uptilted, with the rest remaining downtilted.

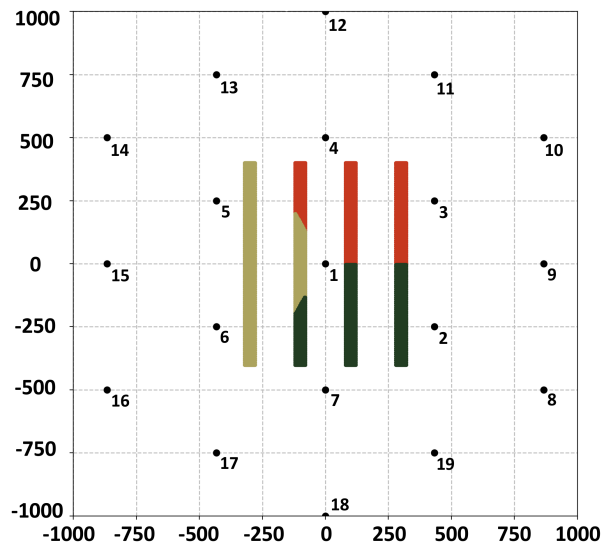
Fig. 3a and Fig. 3b display the cell partitioning for ground users and UAV corridors, respectively, when the vertical tilts θ_i^* are optimized for both populations of end-devices (see case $\alpha = 0.5$ in Fig. 2). The figures show that the optimal tilt arrangement results in BSs 11, 15, and 19 with respective azimuth orientations of 240° , 0° , and 120° , being devoted to covering UAV corridors, with the rest remaining downtilted. The resulting optimal cell partitioning is highly uncustomary and differs from a conventional hexagonal pattern.

Finally, Fig. 4 shows the cumulative distribution function (CDF) of the RSS perceived by ground users (dash-dot line) and UAVs (dash-dash line) when the network is optimized for ground users only ($\alpha = 1$, green), UAVs only ($\alpha = 0$, blue), and both ($\alpha = 0.5$, red). Note that the ground user performance for $\alpha = 1$ (green dash-dot line) and the UAV performance for $\alpha = 0$ (blue dash-dash line) can be regarded as respective upper bounds (in mean) since they entail optimizing all vertical tilts for ground users only and for UAVs only, respectively. Conversely, the ground user performance for $\alpha = 0$ (blue dash-dot line) and the UAV performance for $\alpha = 1$ (green dash-dash line)² can be regarded as respective baselines, obtained when the vertical tilts are chosen ignoring

²Note that the green dash-dash curve exhibits a staircase behavior, explained as follows. For $\alpha = 1$, since tilts are optimized for GUEs only, no cell is pointing its antennas upwards (Fig. 2). UAVs are then just reached by the antenna sidelobe of the respective serving cells, with three cells in total serving all UAVs. All UAVs served by the same cell then experience very similar values of RSS, which are however different for each of the three cells.



(a) Resulting cell partitioning for ground users.



(b) Resulting cell partitioning for UAV corridors.

Fig. 3: Cell partitioning for (a) ground users and (b) UAVs when the vertical tilts are optimized for both (Fig. 2, $\alpha = 0.5$).

ground users and UAVs, respectively. Fig. 4 shows that for $\alpha = 0.5$ the proposed framework reaches a satisfactory tradeoff by: (i) significantly boosting the RSS at UAVs (red dash-dash line) compared to the baseline (green dash-dash line) and approaching the upper bound (blue dash-dash line), and (ii) nearly preserving the RSS at ground users (red dash-dot line) compared to the upper bound (green dash-dot line). While their evaluation falls beyond the scope of this work, both (i) and (ii) may have remarkable positive implications in terms of power control and interference mitigation, achievable rates, and even mobility management [7].

V. CONCLUSION

In this article, we introduced a new mathematical framework for the analysis and design of UAV corridors in cellular

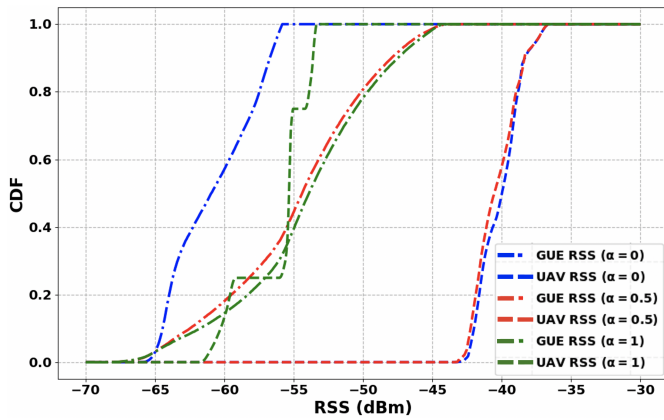


Fig. 4: CDF of the RSS (dBm) at UAVs (dash-dash) and GUEs (dash-dot) when the network is optimized for GUEs only ($\alpha = 1$), UAVs only ($\alpha = 0$), and both ($\alpha = 0.5$).

networks, while considering a realistic network deployment, antenna radiation pattern, and propagation channel model. Our framework, based on quantization theory, allows to optimize the electrical tilts of existing ground cellular base stations to cater for both legacy ground users and UAVs flying along specified aerial corridors. Our case study showed that the ensuing electrical tilt arrangement may result in a highly non-obvious cell partitioning for both ground and UAV users, and that it can boost coverage along UAV corridors without degrading the perceived signal strength on the ground.

Our work is amenable to extensions from at least three standpoints: (i) Rather than focusing on RSS, a proxy for coverage, a similar approach can be taken to optimize for signal-to-interference-plus-noise ratio (SINR). While we found the ensuing analysis to be tractable and insightful, it involves longer mathematical derivations and has been omitted from the present paper due to lack of space; (ii) Our case study assumed LoS condition on all links and a specific antenna arrangement. This could be modified to account for variable (either deterministic or probabilistic) LoS link conditions and to account for other radiation patterns, e.g., with beamformed synchronization signal blocks for initial access; and (iii) Instead of optimizing the antenna tilts for a given cellular deployment, our mathematical framework could be repurposed to optimize the locations of the BSs themselves, to identify suitable sites for dedicated uptilted deployments or both.

REFERENCES

- [1] Y. Zeng *et al.*, *UAV Communications for 5G and Beyond*. Wiley, 2020.
- [2] W. Saad *et al.*, *Wireless Communications and Networking for Unmanned Aerial Vehicles*. Cambridge University Press, 2020.
- [3] K. Namuduri *et al.*, *UAV Networks and Communications*. Cambridge University Press, 2017.
- [4] Q. Wu *et al.*, “A comprehensive overview on 5G-and-beyond networks with UAVs: From communications to sensing and intelligence,” *IEEE J. Sel. Areas Commun.*, vol. 39, no. 10, pp. 2912–2945, 2021.
- [5] C. Diaz Vilor and H. Jafarkhani, “Optimal 3D-UAV trajectory and resource allocation of DL UAV-GE links with directional antennas,” in *Proc. IEEE Globecom*, 2020, pp. 1–6.
- [6] 3GPP Technical Report 36.777, “Study on enhanced LTE support for aerial vehicles (Release 15),” Dec. 2017.
- [7] G. Geraci *et al.*, “What will the future of UAV cellular communications be? A flight from 5G to 6G,” *IEEE Commun. Surveys Tuts.*, vol. 24, no. 3, pp. 1304–1335, 2022.
- [8] A. Garcia-Rodriguez *et al.*, “The essential guide to realizing 5G-connected UAVs with massive MIMO,” *IEEE Commun. Mag.*, vol. 57, no. 12, pp. 84–90, 2019.
- [9] G. Geraci *et al.*, “Understanding UAV cellular communications: From existing networks to massive MIMO,” *IEEE Access*, vol. 6, pp. 67 853–67 865, 2018.
- [10] S. Kang *et al.*, “Millimeter-wave UAV coverage in urban environments,” in *Proc. IEEE Globecom*, 2021.
- [11] C. D’Andrea *et al.*, “Analysis of UAV communications in cell-free massive MIMO systems,” *IEEE Open J. Commun. Society*, vol. 1, pp. 133–147, 2020.
- [12] C. Diaz-Vilor *et al.*, “Cell-free UAV networks: Asymptotic analysis and deployment optimization,” *IEEE Trans. Wireless Commun.*, pp. 1–1, 2022.
- [13] G. Geraci *et al.*, “Integrating terrestrial and non-terrestrial networks: 3D opportunities and challenges,” *arXiv:2207.10385*, 2022.
- [14] M. Mozaffari *et al.*, “Toward 6G with connected sky: UAVs and beyond,” *IEEE Commun. Mag.*, vol. 59, no. 12, pp. 74–80, 2021.
- [15] M. Benzaghta *et al.*, “UAV communications in integrated terrestrial and non-terrestrial networks,” in *Proc. IEEE Globecom*, 2022, pp. 1–6.
- [16] N. Cherif *et al.*, “3D aerial highway: The key enabler of the retail industry transformation,” *IEEE Commun. Mag.*, vol. 59, no. 9, pp. 65–71, 2020.
- [17] A. Bhuyan *et al.*, “Secure 5G network for a nationwide drone corridor,” in *IEEE Aerospace Conference*, 2021, pp. 1–10.
- [18] E. Bulut and I. Guvenc, “Trajectory optimization for cellular-connected UAVs with disconnectivity constraint,” in *Proc. IEEE ICC Workshops*, 2018, pp. 1–6.
- [19] U. Challita *et al.*, “Deep reinforcement learning for interference-aware path planning of cellular-connected UAVs,” in *Proc. IEEE ICC*, 2018, pp. 1–7.
- [20] O. Esrafilian *et al.*, “3D-map assisted UAV trajectory design under cellular connectivity constraints,” in *Proc. IEEE ICC*, 2020, pp. 1–6.
- [21] H. Bayerlein *et al.*, “Multi-UAV path planning for wireless data harvesting with deep reinforcement learning,” *IEEE Open J. Commun. Society*, vol. 2, pp. 1171–1187, 2021.
- [22] S. J. Maeng *et al.*, “Base station antenna uptilt optimization for cellular-connected drone corridors,” *arXiv:2107.00802*, 2021.
- [23] M. M. U. Chowdhury *et al.*, “Ensuring reliable connectivity to cellular-connected UAVs with uptilted antennas and interference coordination,” *ITU J. Future and Evolving Technol.*, 2021.
- [24] S. Singh *et al.*, “Placement of mmWave base stations for serving urban drone corridors,” in *Proc. IEEE VTC-Spring*, 2021, pp. 1–6.
- [25] M. Bernabè *et al.*, “On the optimization of cellular networks for UAV aerial corridor support,” in *Proc. IEEE Globecom*, 2022, pp. 1–6.
- [26] J. Guo and H. Jafarkhani, “Sensor deployment with limited communication range in homogeneous and heterogeneous wireless sensor networks,” *IEEE Trans. Wireless Commun.*, vol. 15, no. 10, pp. 6771–6784, 2016.
- [27] J. Guo *et al.*, “A source coding perspective on node deployment in two-tier networks,” *IEEE Trans. Commun.*, vol. 66, no. 7, pp. 3035–3049, 2018.
- [28] J. Guo and H. Jafarkhani, “Movement-efficient sensor deployment in wireless sensor networks with limited communication range,” *IEEE Trans. Wireless Commun.*, vol. 18, no. 7, pp. 3469–3484, 2019.
- [29] S. Karimi-Bidhendi *et al.*, “Energy-efficient node deployment in heterogeneous two-tier wireless sensor networks with limited communication range,” *IEEE Trans. Wireless Commun.*, vol. 20, no. 1, pp. 40–55, 2020.
- [30] S. Karimi-Bidhendi *et al.*, “Energy-efficient deployment in static and mobile heterogeneous multi-hop wireless sensor networks,” *IEEE Trans. Wireless Commun.*, vol. 21, no. 7, pp. 4973–4988, 2021.
- [31] J. Guo *et al.*, “Optimal deployments of UAVs with directional antennas for a power-efficient coverage,” *IEEE Trans. Commun.*, vol. 68, no. 8, pp. 5159–5174, Aug. 2020.
- [32] E. Koyuncu *et al.*, “Deployment and trajectory optimization of UAVs: A quantization theory approach,” *IEEE Trans. Wireless Commun.*, vol. 17, no. 12, pp. 8531–8546, Dec. 2018.
- [33] 3GPP Technical Report 38.901, “Study on channel model for frequencies from 0.5 to 100 GHz (Release 16),” Dec. 2019.
- [34] I. Goodfellow *et al.*, *Deep learning*. MIT press, 2016.